Biochemical and structural characterization of Roco4

Gilsbach, Bernd

Chapter 5

Structural characterization of LRRK2 Inhibitors

Bernd K. Gilsbach, Ana Messias, Genta Ito, Michael Sattler, Dario Alessi, Alfred Wittinghofer, and Arjan Kortholt

This Chapter has been submitted to: Journal of Medical Chemistry

Structural characterization of LRRK2 Inhibitors

Bernd K. Gilsbach[1], Ana C. Messias[2,3], Genta Ito[4], Michael Sattler[2,3], Dario Alessi[4], Alfred Wittinghofer[5], and Arjan Kortholt[1§]

[1]Department of Cell Biochemistry, University of Groningen, Groningen, The Netherlands

[2]Institute of Structural Biology, Helmholtz Zentrum München, Ingolstädter Landstr. 1, 85764 Neuherberg, Germany

[3]Center for Integrated Protein Science Munich at Biomolecular NMR Spectroscopy, Department Chemie, Technische Universität München, Lichtenbergstr. 4, 85747 Garching bei München, Germany

[4]University of Dundee, Dundee, Scotland

[5]Max-Planck Institut für Molekulare Physiologie, Dortmund, Germany

[§]Correspondence:
Dr. Arjan Kortholt
University of Groningen
Department of Cell Biochemistry
Nijenborgh 7
Groningen, 9747 AG, The Netherlands
A.Kortholt@rug.nl

Abstract

Kinase inhibitors are an important therapeutic target for LRRK2 mediated Parkinson's disease (PD). Many LRRK2 kinase inhibitors have been reported, but none of them can be used for the treatment of LRRK2-mediated PD yet. Here, we show the first co-crystal structures of two commonly used inhibitors, LRRK2-Inh1 and Compound19, with humanized *Dictyostelium* Roco4 kinase and STD-NMR of these inhibitors with the wild type protein. Our data show that humanized Roco4 can serve as excellent tool for the structural characterization and optimization of LRRK2 inhibitors using X-ray Crystallography and NMR Spectroscopy.

Introduction

Parkinson´s disease (PD) is the second most common neurodegenerative disorder and is affecting 2 % of the population above 65 years [1]. Genome-wide association screens revealed that several missense mutations in the LRRK2 gene are found both in hereditary and sporadic Parkinson´s disease [2–4]. LRRK2 is a large multi-domain protein that belongs to the Roco family of G-proteins. LRRK2 consists of N-terminal Armadillo, ankyrin and LRR repeats followed by a small GTPase like domain called Roc (Ras of complex proteins), a COR (C-terminal of Roc), a kinase and a WD40 domain. Mutations are found in nearly every domain of LRRK2 and several have been linked to increased kinase and decreased GTPase activity, suggesting a gain of function mechanism [5]. The most prevalent G2019S mutation is located in the kinase domain and leads to a 2-4 fold increase in kinase activity [6–9]. Therefore, the major focus of the pharmaceutical industry has been to develop kinase inhibitors as potential therapeutics. Several LRRK2 inhibitors have been reported, but many of the them lack selectivity or the capability to pass the blood brain barrier [10–15]. Furthermore the recent published LRRK2 specific and brain penetrant inhibitors lead to kidney and lung abnormality. Hence, though the current kinase inhibitors cannot be used for the treatment of LRRK2-mediated PD, they are being used as important tool to characterize the function and activation mechanism of LRRK2 [16–20].

Structural understanding of LRRK2 has come mainly from studies using Roco proteins from lower organisms[21,22]. Importantly, our structure of the *Dictyostelium* Roco4 kinase domain showed that the increased kinase activity of LRRK2(G2019S) is caused by an additional hydrogen bond between the mutated Ser and residue Gln1918 (Arg1077 in Roco4) coming from the αC-helix, which stabilizes the active kinase conformation[22].

In this study, we generated humanized *Dictyostelium* Roco4 kinase protein and used this subsequently together the wild type kinase as tool to characterize biochemically and structurally LRRK2 specific inhibitors at a molecular level.

Results

Designing and characterization of Humanized Roco4

Our previously identified structure of the Roco4 kinase in complex with the rather unspecific LRRK2 inhibitor H1152 showed that *Dictyostelium* Roco4 kinase can be used as an important tool to biochemically and structurally characterize the LRRK2 kinase, its mutations and possibly binding of inhibitors[22]. However, all attempts to crystallize more specific LRRK2 inhibitors failed: co-crystallization of Roco4 kinase with LRRK2-Inh1 and Compound19 led to apo crystal structures. This suggests that Roco4 has a much lower affinity for these inhibitors compared to LRRK2. We therefore analyzed inhibitor binding to Roco4 kinase with Saturation Transfer Difference (STD) NMR[24,25], which can detect binding of small ligands to macromolecules with dissociation constants K_D ranging from nM to mM. STD NMR is based on the transfer of saturation of magnetization from the protein to the bound ligand(s), which mediated by exchange of free and bound ligand is detected with the NMR signals of the ligand. A subtraction of this spectrum from a spectrum without protein saturation reflects NMR signals of ligands that are in contact with the protein in the bound state. Ligand protons closer to the protein in the binding interface show the most intense STD NMR signals. An extension of this method, named ATP-STD NMR, has been developed for screening of protein kinases[26]. ATP-STD competition experiments with equimolar concentration of ATP and LRRK2-Inh1 and Compound19 showed that both inhibitors compete with ATP for the Roco4 ATP-binding pocket (Fig. 1A + B). This shows that LRRK2-Inh1 and Compound19 are both able to bind to Roco4. However, competition of these inhibitors with ATP show signals from both ATP and the inhibitors simultaneously, indicating that the affinity of the inhibitors and thus the IC50 to wild-type (wt) Roco4 kinase must be low (ATP binds typically to kinases with a K_D of 10-100 µM). Consistently, kinase activity assays showed that LRRK2-Inh1 and Compound19 inhibit wt Roco4 kinase with an IC50 of 1278 µM and 240 µM respectively (Fig. 1C).

Although the anticipated binding pocket of LRRK2 inhibitors in the ATP binding site is reasonably well conserved between Roco4 and LRRK2, modeling of one of the LRRK2 specific inhibitors (LRRK2-Inh1) into the binding pocket revealed that two Phe of Roco4

would clash with inhibitor binding (Fig. 1D). Mutants, in which one or both of these residues (Phe1107 and Phe1161) of Roco4 were mutated to leucine, were generated. Introducing these mutations does not affect the kinase activity of the protein (V_{max}, K_m(ATP)), but led to a decrease of the IC50 values for LRRK2-Inh1 and Compound 19: the IC50 for LRRK2-Inh1 drops from 933 µM to 68 µM for the single and 5.3 µM for the double mutant and for Compound 19 from 240 µM to 89 µM for the single and 15.4 µM for the double mutant (Fig. 1C). This almost 175 fold preference of LRRK2-Inh1 and 15 fold preference of compound19 for the double mutant Roco4(F1107L/F1161L) (referred to as humanized Roco4 from now on) compared to wild-type kinase is thus considered a very valuable tool for detailed structural and biochemical characterization of LRRK2 inhibitor binding.

Structural characterization of LRRK2-Inh1 binding

LRRK2-Inh1 is the first identified LRRK2 specific inhibitor and is now a common tool compound for the LRRK2 research community. LRRK2-Inh1 has a 2-amino-5, 11-dimethyl-5H-benzo[e]pyrimido-[5,4-b][1,4]diazepine-6(11H)-one scaffold and inhibits LRRK2 with an IC50 value of 13 nM to wt and 6 nM to the G2019S mutation. LRRK2-Inh1 showed high selectivity against a panel of more than 470 kinases and is able to lead to the dephosphorylation of LRRK2 residues Ser910 and Ser935 in kidney but not in brain of mice, indicating that it is not capable of crossing the blood-brain-barrier[10].

Humanized Roco4 kinase containing the LRRK2-Inh1 inhibitor crystallized in space group $P2_12_12_1$ and diffracted up to 3.0 Å with two molecules in the asymmetric unit cell. The density map was refined to a R_{work}/R_{free} of 0.25 and 0.30, respectively. The r.m.s.d. between the wt and the inhibitor structure is 1.65 Å. The structure of the humanized kinase has the typical kinase fold and does not differ much from the wt structure (Fig. 2A). It shows the typical kinase fold with a more β-sheet containing N-terminal lobe and an α-helical C-terminal lobe. The cleft between these lobs forms the ATP binding pocket. Kinase inhibitors which bind in the ATP binding pocket of protein kinases have been classified as type 1 and type 2. Type 1 molecules recognize specifically the active, while type 2 inhibitors bind specifically to the inactive conformation, with additional interactions involving the DFG loop[27]. The major difference between the structure of active Roco4 kinase and inactive Roco4 kinase is the conformation of the activation loop: in the inactive state this loop is disordered, while in the phosphorylated state it reorients into an ordered active conformation[23].

While LRRK2-Inh1 is predicted to be a type1 inhibitor our crystal structure suggests that it does not strictly stabilize the active conformation: the activation loop is poorly resolved indicating that it is flexible[22]. The strongest difference between the apo and LRRK2-Inh1 structures is the closure of the glycine-rich loop in the inhibitor structure. It is moved towards the C-terminal lobe by ~5Å and covers the phosphate binding sites. The buried surface area is 530 $Å^2$ and the inhibitor makes two hydrogen bonds and 24 van der Waals contacts with the kinase. The hydrogen bonds are formed between the backbone carbonyl of Val1055 (hinge region) and the N24 of the inhibitor with a distance of 2.8Å (3.1 Å in the other molecule) and Lys1055 and O40 with a distance of 3.2 Å (3.8 Å in the other molecule) (Fig. 2B). Lys 1055 is the conserved Lys from β-strand 3 (PKA: Lys72) which forms a hydrogen bond with a conserved Glu 1078 (PKA: Glu91) coming from the αC-helix. The heterocyclic ring system of the LRRK2 inhibitor is accommodated by the adenine binding pocket of Roco4, the adjacent phenolic ring is partly covered by the hinge region and the other part of the inhibitor points into the solvent The electron density of the methyl-4-(piperidine-4-yl)-piperazine moiety of the molecule is weak (Fig. 2B + C), suggesting that it is exposed to the solvent, flexible and unlikely to contribute to binding. In STD NMR experiments with the WT kinase (Figure 1A) we observe STD signals with all protons of Inh-1 except the piperazine-piperidine protons. Accordingly inhibitor protons closer to the protein binding interface, i.e. the pyrimido H29 and the diazepine methyl H41 protons, which are in-between the two above referred inhibitor-kinase hydrogen bonds (N24 (Ihn-1) – O(Val1055) and O40(Inh-1) – Nz(Lys1055)), exhibit stronger STD signals. These observations are fully consistent with the crystal structure of the humanized kinase with Inh-1.

Structural characterization of Compound 19 binding

Compound19 is a type 1 inhibitor derived from a diaminopyrimidine scaffold and is able to cross the blood-brain-barrier. Compound 19 has an IC50 of 4 nM to wt LRRK2 and only showed inhibition greater than 50% of TTK protein kinase at 0.1 µM when screened against a panel 187 kinases [12]. The inhibitor Compound 19 co-crystallized with the humanized kinase domain of Roco4 in space group $P4_32_12$ and diffracted to a resolution of 1.55 Å .The density map was refined to a Rwork/Rfree of 0.19 and 0.21 respectively. The r.m.s.d. between the apo and the inhibitor structure is 0.97 Å. In contrast to the LRRK2-Inh1 structure, the activation loop is resolved indicating that it is less flexible and that Compound19 only bind and

stabilizes the active conformation. There is a slight closure of the glycine-rich loop; it is moved 2Å towards the C-terminal lobe (Fig. 3A). The inhibitor covers an area of 439 $Å^2$. The pyrimidine ring and the C5 trifluoromethyl and C6 aminocyclopropyl cover the adenine binding pocket. The amino N15 of the inhibitor forms a hydrogen bond with the carbonyl of Val1055 of the hinge region. Furthermore the inhibitor makes 20 van der Waals contacts. In addition to the direct contacts two water molecules are recognized in the crystal structure which create a hydrogen bond network between the fluorides of the inhibitor and the head groups of Asp1177 (D of the DFG motive) and Glu1078 (αC-helix) (Fig. 3B). Since there are two conformations visible for Asp1177, one which is in the correct distance to the connecting water and one which is too far away (5Å) it is likely that this interaction does not add much to the binding energy of the inhibitor. The C25 morpholino part is pointing into the solvent and has no electron density, indicated by the elevated B-factors of this part, suggesting this group is flexible and does not bind to the kinase domain (Fig. 3 B + C). In agreement with the crystal structure of the humanized kinase with Compound 19, we observe on STD experiments with the WT kinase (Figure 1B), STD signals with all protons of Compound 19 except the morpholino protons. Moreover, the compound protons closer to the protein binding interface show stronger STD signals: the protons closer to the hinge region (the pyrimidine H4 and the phenyl methoxy and H20 protons) and the N-lobe ß-strands (the cyclopropyl protons).

Discussion and Conclusions

Although the kinase domain of Roco4 and LRRK2 are quite similar we were unable to co-crystallize LRRK2 specific inhibitors with Roco4, consistent with a previous study of Liu et al., [20]. However, in contrast to Liu et al., we were able to generate humanized Roco4 kinase that efficiently binds to inhibitors. Mutation of two Phe to Leu in the catalytic site, one in the hinge region and one in β strand 6, does not change the overall fold or activity of the protein, but decreased the IC50 values for LRRK2 inhibitors dramatically. The co-structures of humanized Roco4 with both LRRK2-Inh1 and Compound 19, revealed no major difference in the overall fold with the wt AppCp Roco4 structure (Fig S1). The largest difference is the closure of the glycine-rich loop. Furthermore the visibility of the activation loop in the Compound19 structure indicates that this compound is clearly type1 whereas LRRK2-Inh1

also might bind to the inactive conformation of the kinase. Both inhibitors bind in a highly similar way and make contact to the same position in the hinge region and to the conserved Lys from β3 (in the Compound19 structure mediated by a water molecule). Thus, it is rather unlikely that LRRK2 specificity is archived by polar interaction but rather by the non-polar and van der Waals interactions. Importantly, the structures and the STD-NMR data show that the long tail of both inhibitors is not making contact with the protein and sticking out of the binding pocket, and thus can be used for improvement of these inhibitors. Optimization of the current and identification of new LRRK2 inhibitors is urgently needed to efficiently target LRRK2-mediated PD. Our data show that humanized Roco4 kinase can be used as important tool in this enterprise.

Experimental section

Expression of humanized Roco4 kinase

Roco4 kinase (amino acids 1018– 1292) was cloned into a Gateway-compatible pGEX4T1 plasmid containing an N-terminal TEV cleavage side. The two point mutations were introduced by the Quick Change method. Proteins were purified in the presence of 1 mM ATP by GSH affinity, cleavage, and size-exclusion chromatography.

NMR Spectroscopy

NMR experiments were recorded on a 800 MHz spectrometer equipped with a TXI probehead at 298 K using 10 μM Roco4 kinase in 20mM deuterated Tris.HCl pH 8, 300 mM NaCl, 10mM $MgCl_2$, 1.15 mM deuterated DTT, 0.002% NaN_3 (90% H_2O / 10% D_2O). 1D proton experiments were performed using a WATERGATE pulse sequence with 32k time domain points and 64 scans. STD experiments were recorded using an interleaved pulse program with on-resonance protein irradiation at 0.75 ppm (LRRK2-Inh1) or 1.6 ppm (Compound 19), and off-resonance irradiation at –5 ppm with 4s total effective irradiation, using 2048 scans and 32k time domain points. Competition experiments were performed using equimolar concentrations of AMP-PNP and inhibitor: 506 μM AMP-PNP and 506μM LRRK2-Inh1 or 509 μM AMP-PNP and 509μM Compound19 respectively. Spectra were processed using TOPSPIN 3.2.

IC50 measurements

Roco4 kinase activity was determined at 30 °C in kinase buffer consisting of 50 mM Tris-HCl pH 7.5, 0.1 mM EGTA, 25 μM [γ-^{32}P]ATP (~300 cpm/pmol), 10 mM $MgCl_2$, 2 mM DTT and 150 μM LRRKtide. The reaction was started by adding Roco4 and was stopped after 5 min by spotting samples on P81 phosphocellulose papers and washing them with 50 mM phosphoric acid. The P81 papers were washed once in acetone and dried before scintillation counting. The assays were performed with 0.040 mg/mL kinase and kinase inhibition was determined by varying the concentration of inhibitor.

Crystallography

Roco4 crystals were obtained in 100 mM 1,3-bis(tris (hydroxymethyl)methylamino)propane (pH 8,5), 200 mM Na/K tartrate, and 11% (wt/vol) PEG 3350 using the hanging drop/vapor diffusion method in the presence of 2 mM inhibitor. For data collection, crystals were cryoprotected in reservoir solution containing 20% (wt/vol) Glycerol as cryoprotectant. Datasets were collected on beam line ×10SA at the Swiss Light Source (Paul Scherrer Institut, Villigen, Switzerland) and were indexed, integrated, and scaled with the XDS package. Both inhibitor structures were solved by molecular replacement using the wt Roco4 structure (PDB: 4F0G) as the search model. The model was built in COOT and refined with REFMAC5 using TLS- refinement (CCP4 suite). Figures were generated using PYMOL (DeLano Scientific LLC).

Acknowledgement

This work is part of the Michael J. Fox Foundation LRRK2 Biological Structure and Function consortium and AK is funded by an NWO-VIDI grant

References:

(1) Lees, A. J.; Hardy, J.; Revesz, T. Parkinson's Disease. *Lancet* **2009**, *373*, 2055–2066.

(2) Satake, W.; Nakabayashi, Y.; Mizuta, I.; Hirota, Y.; Ito, C.; Kubo, M.; Kawaguchi, T.; Tsunoda, T.; Watanabe, M.; Takeda, A.; Tomiyama, H.; Nakashima, K.; Hasegawa, K.; Obata, F.; Yoshikawa, T.; Kawakami, H.; Sakoda, S.; Yamamoto, M.; Hattori, N.; Murata, M.; Nakamura, Y.; Toda, T. Genome-Wide Association Study Identifies Common Variants at Four Loci as Genetic Risk Factors for Parkinson's Disease. *Nat. Genet.* **2009**, *41*, 1303–1307.

(3) Zimprich, A.; Biskup, S.; Leitner, P.; Lichtner, P.; Farrer, M.; Lincoln, S.; Kachergus, J.; Hulihan, M.; Uitti, R. J.; Calne, D. B.; Stoessl, a J.; Pfeiffer, R. F.; Patenge, N.; Carbajal, I. C.; Vieregge, P.; Asmus, F.; Müller-Myhsok, B.; Dickson, D. W.; Meitinger, T.; Strom, T. M.; Wszolek, Z. K.; Gasser, T. Mutations in LRRK2 Cause Autosomal-Dominant Parkinsonism with Pleomorphic Pathology. *Neuron* **2004**, *44*, 601–607.

(4) Paisán-Ruíz, C.; Jain, S.; Evans, E. W.; Gilks, W. P.; Simón, J.; van der Brug, M.; López de Munain, A.; Aparicio, S.; Gil, A. M.; Khan, N.; Johnson, J.; Martinez, J. R.; Nicholl, D.; Carrera, I. M.; Pena, A. S.; de Silva, R.; Lees, A.; Martí-Massó, J. F.; Pérez-Tur, J.; Wood, N. W.; Singleton, A. B. Cloning of the Gene Containing Mutations That Cause PARK8-Linked Parkinson's Disease. *Neuron* **2004**, *44*, 595–600.

(5) Gilks, W. P.; Abou-Sleiman, P. M.; Gandhi, S.; Jain, S.; Singleton, A.; Lees, A. J.; Shaw, K.; Bhatia, K. P.; Bonifati, V.; Quinn, N. P.; Lynch, J.; Healy, D. G.; Holton, J. L.; Revesz, T.; Wood, N. W. Common LRRK2 Mutation in Idiopathic Parkinson's Disease. *Lance* **2005**, *365*, 415–416.

(6) Anand, V. S.; Reichling, L. J.; Lipinski, K.; Stochaj, W.; Duan, W.; Kelleher, K.; Pungaliya, P.; Brown, E. L.; Reinhart, P. H.; Somberg, R.; Hirst, W. D.; Riddle, S. M.; Braithwaite, S. P. Investigation of Leucine-Rich Repeat Kinase 2 : Enzymological Properties and Novel Assays. *FEBS J.* **2009**, *276*, 466–478.

(7) West, A. B.; Moore, D. J.; Biskup, S.; Bugayenko, A.; Smith, W. W.; Ross, C. A.; Dawson, V. L.; Dawson, T. M. Parkinson ' S Disease-Associated Mutations in Leucine-Rich Repeat Kinase 2 Augment Kinase Activity. *PNAS* **2005**.

(8) Greggio, E.; Jain, S.; Kingsbury, A.; Bandopadhyay, R.; Lewis, P.; Kaganovich, A.; van der Brug, M. P.; Beilina, A.; Blackinton, J.; Thomas, K. J.; Ahmad, R.; Miller, D. W.; Kesavapany, S.; Singleton, A.; Lees, A.; Harvey, R. J.; Harvey, K.; Cookson, M. R. Kinase Activity Is Required for the Toxic Effects of Mutant LRRK2/dardarin. *Neurobiol. Dis.* **2006**, *23*, 329–341.

(9) Jaleel, M.; Nichols, R. J.; Deak, M.; Campbell, D. G.; Gillardon, F.; Knebel, A.; Alessi, D. R. LRRK2 Phosphorylates Moesin at Threonine-558: Characterization of How Parkinson's Disease Mutants Affect Kinase Activity. *Biochem. J.* **2007**, *405*, 307–317.

(10) Deng, X.; Dzamko, N.; Prescott, A.; Davies, P.; Liu, Q.; Yang, Q.; Lee, J.-D.; Patricelli, M. P.; Nomanbhoy, T. K.; Alessi, D. R.; Gray, N. S. Characterization of a Selective Inhibitor of the Parkinson's Disease Kinase LRRK2. *Nat. Chem. Biol.* **2011**, *7*, 203–205.

(11) Reith, A. D.; Bamborough, P.; Jandu, K.; Andreotti, D.; Mensah, L.; Dossang, P.; Choi, H. G.; Deng, X.; Zhang, J.; Alessi, D. R.; Gray, N. S. GSK2578215A; a Potent and Highly Selective 2-Arylmethyloxy-5-Substitutent-N-Arylbenzamide LRRK2 Kinase Inhibitor. *Bioorg. Med. Chem. Lett.* **2012**, *22*, 5625–5629.

(12) Estrada, A. a; Liu, X.; Baker-Glenn, C.; Beresford, A.; Burdick, D. J.; Chambers, M.; Chan, B. K.; Chen, H.; Ding, X.; DiPasquale, A. G.; Dominguez, S. L.; Dotson, J.; Drummond, J.; Flagella, M.; Flynn, S.; Fuji, R.; Gill, A.; Gunzner-Toste, J.; Harris, S. F.; Heffron, T. P.; Kleinheinz, T.; Lee, D. W.; Le Pichon, C. E.; Lyssikatos, J. P.; Medhurst, A. D.; Moffat, J. G.; Mukund, S.; Nash, K.; Scearce-Levie, K.; Sheng, Z.; Shore, D. G.; Tran, T.; Trivedi, N.; Wang, S.; Zhang, S.; Zhang, X.; Zhao, G.; Zhu, H.; Sweeney, Z. K. Discovery of Highly Potent, Selective, and Brain-Penetrable Leucine-Rich Repeat Kinase 2 (LRRK2) Small Molecule Inhibitors. *J. Med. Chem.* **2012**, *55*, 9416–9433.

(13) Chen, H.; Chan, B. K.; Drummond, J.; Estrada, A. a; Gunzner-Toste, J.; Liu, X.; Liu, Y.; Moffat, J.; Shore, D.; Sweeney, Z. K.; Tran, T.; Wang, S.; Zhao, G.; Zhu, H.; Burdick, D. J. Discovery of Selective LRRK2 Inhibitors Guided by Computational Analysis and Molecular Modeling. *J. Med. Chem.* **2012**, *55*, 5536–5545.

(14) Yun, H.; Heo, H. Y.; Kim, H. H.; Dookim, N.; Seol, W. Identification of Chemicals to Inhibit the Kinase Activity of Leucine-Rich Repeat Kinase 2 (LRRK2), a Parkinson's Disease-Associated Protein. *Bioorg. Med. Chem. Lett.* **2011**, *21*, 2953–2957.

(15) Ramsden, N.; Perrin, J.; Ren, Z.; Lee, B. D.; Zinn, N.; Dawson, V. L.; Tam, D.; Bova, M.; Lang, M.; Drewes, G.; Bantscheff, M.; Bard, F.; Dawson, T. M.; Hopf, C. Chemoproteomics-Based Design of Potent LRRK2-Selective Lead Compounds That Attenuate Parkinson's Disease-Related Toxicity in Human Neurons. *ACS Chem. Biol.* **2011**, 0–7.

(16) Kramer, T.; Monte, F. Lo; Go, S.; Marlyse, G.; Amombo, O.; Schmidt, B. Small Molecule Kinase Inhibitors for LRRK2 and Their Application to Parkinson's Disease Models. **2012**.

(17) Ray, S.; Liu, M. Current Understanding of LRRK2 in Parkinson ' S Disease : Biochemical and Structural Features and Inhibitor Design. **2004**, 1701–1713.

(18) Göring, S.; Taymans, J.-M.; Baekelandt, V.; Schmidt, B. Indolinone Based LRRK2 Kinase Inhibitors with a Key Hydrogen Bond. *Bioorg. Med. Chem. Lett.* **2014**, *24*, 4630–4637.

(19) Henderson, J. L.; Kormos, B. L.; Hayward, M. M.; Coffman, K. J.; Jasti, J.; Kurumbail, R. G.; Wager, T. T.; Verhoest, P. R.; Noell, G. S.; Chen, Y.; Needle, E.; Berger, Z.; Steyn, S. J.; Houle, C.; Hirst, W. D.; Galatsis, P. Discovery and Preclinical Profiling of

3-[4-(morpholin-4-Yl)-7H-pyrrolo[2,3-D]pyrimidin-5-Yl]benzonitrile (PF-06447475), a Highly Potent, Selective, Brain Penetrant, and in Vivo Active LRRK2 Kinase Inhibitor. *J. Med. Chem.* **2014**.

(20) Liu, Z.; Galemmo, R. a; Fraser, K. B.; Moehle, M. S.; Sen, S.; Volpicelli-Daley, L. a; DeLucas, L. J.; Ross, L. J.; Valiyaveettil, J.; Moukha-Chafiq, O.; Pathak, A. K.; Ananthan, S.; Kezar, H.; White, E. L.; Gupta, V.; Maddry, J. a; Suto, M. J.; West, A. B. Unique Functional and Structural Properties of the LRRK2 ATP-Binding Pocket. *J. Biol. Chem.* **2014**.

(21) Gotthardt, K.; Weyand, M.; Kortholt, A.; Van Haastert, P. J. M.; Wittinghofer, A. Structure of the Roc-COR Domain Tandem of C. Tepidum, a Prokaryotic Homologue of the Human LRRK2 Parkinson Kinase. *EMBO J.* **2008**, *27*, 2239–2249.

(22) Gilsbach, B. K.; Ho, F. Y.; Vetter, I. R.; van Haastert, P. J. M.; Wittinghofer, A.; Kortholt, A. Roco Kinase Structures Give Insights into the Mechanism of Parkinson Disease-Related Leucine-Rich-Repeat Kinase 2 Mutations. *Proc. Natl. Acad. Sci. U. S. A.* **2012**, *109*, 10322–10327.

(23) Kornev, A. P.; Haste, N. M.; Taylor, S. S.; Eyck, L. F. Ten. Surface Comparison of Active and Inactive Protein Kinases Identifies a Conserved Activation Mechanism. *Proc. Natl. Acad. Sci. U. S. A.* **2006**, *103*, 17783–17788.

Figure Legend:

Fig.1: STD NMR and IC50 measurement. A. STD signals from LRRK2-Inh1 and AMP-PNP protons indicate binding of both LRRK2-Inh1 and AMP-PNP to Roco4 kinase. In the 1D spectrum (blue) protons from AMP-PNP are indicated, whilst in the STD spectrum (red) the proton H29 from LRRK2-Inh1 is indicated. Chemical structure of LRRK2-Inh proton H29 is indicated by a red circle B. STD signals from Compound19 and AMP-PNP protons indicate binding of both Compound19 and AMP-PNP to Roco4 kinase. In the 1D spectrum (blue) protons from AMP-PNP are indicated, whilst in the STD spectrum (red) the pyrimidine proton H4, and the phenyl protons H17 and H20 from Compound19 are indicated. Chemical structure of Compound19 protons H4, H17 and H20 are indicated by a red circles C. IC50 measurement with increasing concentration of LRRK2-Inh1 and Compound19. D. Detailed view of the LRRK2-Inh1 bound to the humanized Roco4 kinase. The two mutated F to L are indicated in red.

Fig.2: Co-crystal structure of Roco4 kinase and LRRK2-Inh1 A. Overlay of the AppCp (blue) with the LRRK2-Inh1 (green) structure. B. Close-up of the inhibitor binding pocket. Hydrogen bonds indicated by dashed line. C. Structure of LRRK2-Inh1. Observed electron density indicated by mesh.

Fig.3: Co-crystal structure of Roco4 kinase and Compound19 A. Overlay of the AppCp (blue) with the Compound19 (green) structure. B. Close-up of the inhibitor binding pocket. Hydrogen bonds indicated by dashed line, waters shown as spheres (red). C. Structure of Compound19. Observed electron density indicated by mesh.

Sup.1: Overlay of Roco4 bound to AppCp (PDB: 4F0F; orange), bound to LRRK2-In1 (PDB: XXXX; blue), bound to Compound19 (PDB: XXXX; green).

Fig. 1:

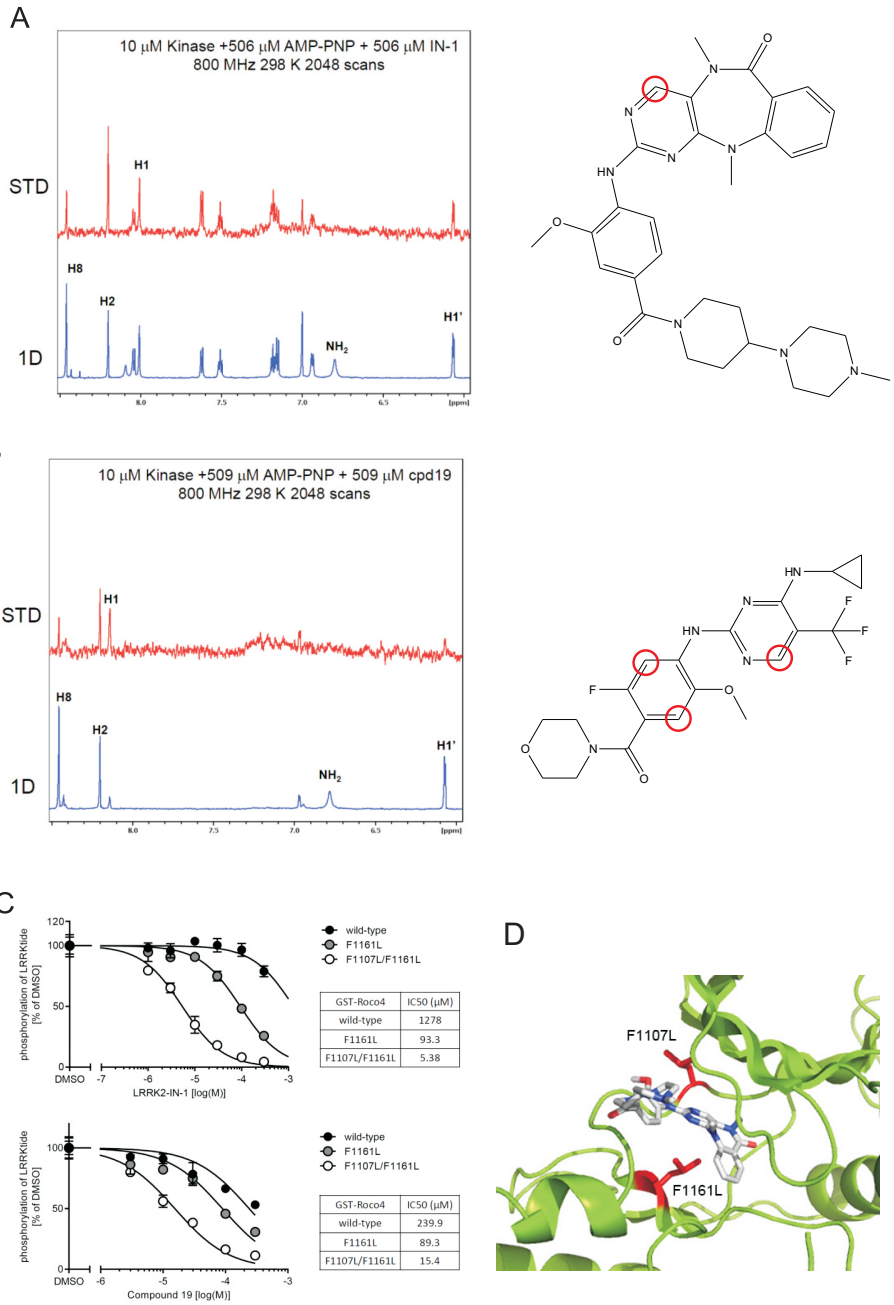
A
10 µM Kinase +506 µM AMP-PNP + 506 µM IN-1
800 MHz 298 K 2048 scans
STD
1D
H1
H8
H2
H1'
NH2
B
10 µM Kinase +509 µM AMP-PNP + 509 µM cpd19
800 MHz 298 K 2048 scans
STD
1D
H1
H8
H2
H1'
NH2
C
phosphorylation of LRRKtide [% of DMSO]
LRRK2-IN-1 [log(M)]
wild-type
F1161L
F1107L/F1161L
GST-Roco4 | IC50 (µM)
wild-type | 1278
F1161L | 93.3
F1107L/F1161L | 5.38
Compound 19 [log(M)]
GST-Roco4 | IC50 (µM)
wild-type | 239.9
F1161L | 89.3
F1107L/F1161L | 15.4
D
F1107L
F1161L

Fig. 2:

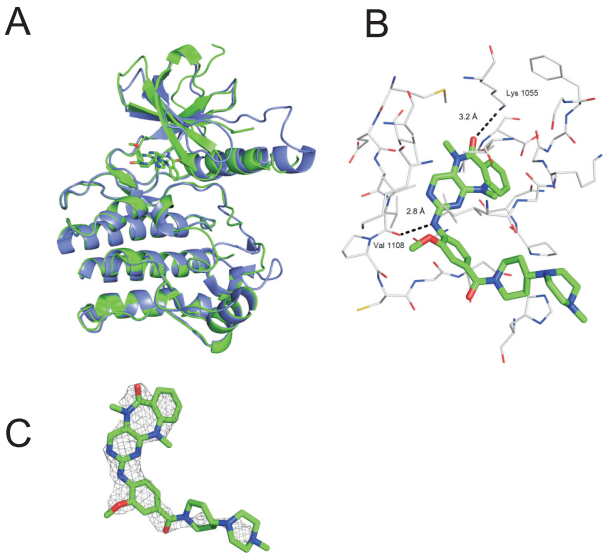

Fig. 3:

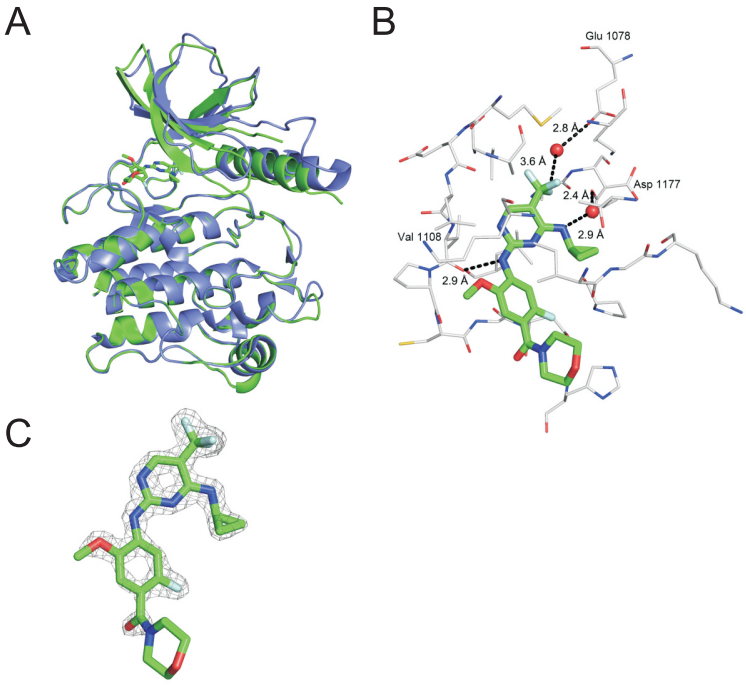

Sup. 1:

A

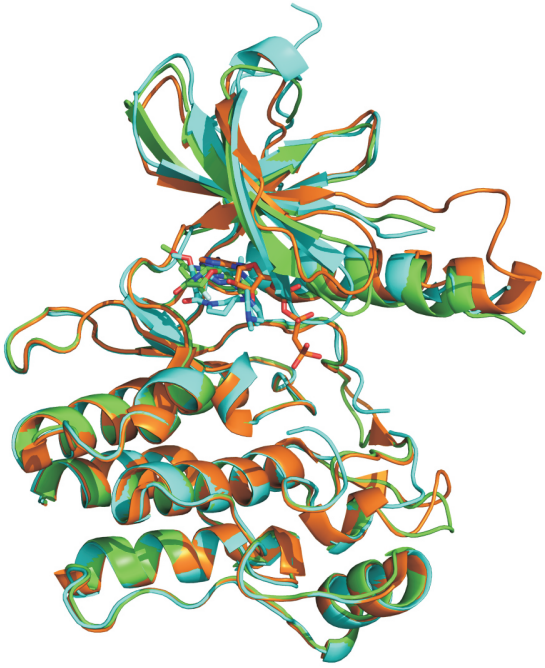

Appendix to Chapter 5; unpublished inhibitor structures:

The recently identified LRRK2 inhibitors, HG-10-102-01 and GNE-7915 are selective and brain penetrant [21–23]. However, long-term inhibition of LRRK2 with these inhibitors leads, similar to disrupting LRRK2 in mice, to kidney abnormality [23-25]. Developing kinase inhibitors specific to PD mutants of LRRK2, not affecting wild-type, might therefore be the most promising approach. We are therefore currently, in collaboration with Dr. Gray/Dr. Alessi, using the humanize Roco4 kinase for co-crystallizing and optimizing a set of inhibitors that are more specific for PD-mutated LRRK2 (Thesis Chapter 5).

Structural characterization of HG 09-106-03 and HG 09-105-05

The inhibitors HG 09-106-03 and HG 09-105-05 are a new class of LRRK2 inhibitors that are derived from a N2, N4-diphenylpyrimidine-2,4-diamine. Biochemical experiments showed that HG 09-106-03 and HG 09-105-05 are ~40 fold more potent against LRRK2 carrying the PD mutations: HG 09-106-03 and HG 09-105-05 inhibit wt LRRK2 with an IC50 of 20.4 nM and 12.9 nM respectively, while they inhibit the G2019S mutant form of LRRK2 with an IC50 of 0.5 nM and 0.2 nM (Fig. 1). To further optimize and characterize these inhibitors we co-crystallized both with our "humanized" Roco4 kinase model (Thesis Chapter 5). The inhibitors HG 09-106-03 and HG 09-105-05 both co-crystallized with the humanized Roco4 kinase domain in space group $P4_32_12$ and diffracted to 1.6 Å and 1.8 Å, respectively. The structure was refined to a R_{work}/R_{free} of 0.19/0.22 and 0.22/0.25. The r.m.s.d. between the inhibitor structures is 0.85 $Å^2$ and 0.95 $Å^2$ for HG 09-106-03 and HG 09-105-05 respectively. During refinement it was striking that the activation loop had good electron density, which was completely different to all other Roco4 kinase structures solved so far indicating that it is in more fixed state in the inhibitor bound state and less flexible. There is a slight closure of the glycine-rich loop in both structures: it is moved 1.7 Å in the HG 09-106-03 and 2.1 Å in the HG 09-105-05 structure towards the C-terminal lobe (Fig. 2a + 3a). The inhibitors cover nearly the same area 523 $Å^2$ and 545 $Å^2$. The 2-(isopropylsulfonyl)phenyl)pyrimidine-2,4-diamine part covers the adenine binding pocket, the anisole makes contact with the hinge region and the morpholine part points into the solvent. Both inhibitors form two hydrogen bonds between Val 1108 and N20 and Lys1055 and O9 with comparable distances of 2.7 Å /

2.8 Å and 3.4 Å / 3.3 Å respectively (Fig. 2b + 3c). Besides the two hydrogen bonds HG 09-106-03 and HG 09-105-05 make 23 van der Waals contacts. The tail of both inhibitors is not visible in the structure and most likely do not contribute to binding (Fig 2c/d + 3c/d). To test this we synthesized a shorter version of the HG 09-106-03 not containing the side chain. This shorter compound showed the same IC 50 towards LRRK2, indicating that the tail does not contribute to the inhibitory capability of the HG 09-106-03 and HG 09-105-05 and thus can be used for optimization of solubility or improve the ability to cross the blood brain barrier of these compounds.

Outlook

The obtained structures do not provide a simple explanation for the higher affinity of the HG 09-106-03 and HG 09-105-05 to the mutant G2019S form of LRRK2 compared to wt LRRK2. In both structures the inhibitor is 8 Å away from the side of the PD-mutation. However, in the structures of the G2019S specific inhibitors the activation loop was completely in the active conformation. Therefore, we speculate that these inhibitors strongly favor binding to the active conformation over the inactive conformation. The PD mutation have a higher activity, and thus are more in the active state, which would explain the preference of these inhibitors for PD-mutated LRRK2. Alternatively, since a part of the inhibitor points into the solved, other parts of LRRK2 might be involved in binding of these inhibitors. Pull-down and activity studies revealed that the Roco4 LRRs bind to and regulates Roco4 kinase activity. Furthermore, cross-linking data on full-length LRRK2 showed that the N-terminus might interact with the kinase at the activation loop and the hinge region between the N- and C-terminal lobes and thereby directly interferes with inhibitor binding. Currently studies are in progress with both full-length and N-terminal truncated LRRK2 protein to test the proposed mechanisms for PD specificity in more detail.

Materials and Methods

IC50 measurements

Active GST-LRRK2 (1326-2527), GST-LRRK2 [G2019S] (1326-2527), GST-LRRK2 [A2016T] (1326-2527), GST-LRRK2 [I2020T] (1326-2527) and GST-LRRK2[A2016T+G2019S] (1326-2527) enzyme was purified with glutathione sepharose

from HEK293 cell lysate 36 h following transient transfection of the appropriate cDNA constructs as described previously. Peptide kinase assays, performed in duplicate, were set up in a total volume of 40 µl containing 0.5 µg LRRK2 kinase (which at approximately 10% purity gives a final concentration of 8 nM) in 50 mM Tris/HCl, pH 7.5, 0.1 mM EGTA, 10 mM MgCl2, 20 µM Nictide, 0.1 µM [γ-32P]ATP (~500 cpm/pmol) and the indicated concentrations of inhibitor dissolved in DMSO. After incubation for 15 min at 30 °C, reactions were terminated by spotting 35 µl of the reaction mix onto P81 phosphocellulose paper and immersion in 50 mM phosphoric acid. Samples were washed extensively and the incorporation of [γ-32P]ATP into Nictide was quantified by Cerenkov counting. IC50 values were calculated with GraphPad Prism using non-linear regression analysis.

Crystallography

Roco4 crystals were obtained in 100 mM 1,3-bis(tris (hydroxymethyl)methylamino)propane (pH 8,5), 200 mM Na/K tartrate, and 11% (wt/vol) PEG 3350 using the hanging drop/vapor diffusion method in the presence of 2 mM inhibitor. For data collection, crystals were cryoprotected in reservoir solution containing 20% (wt/vol) Glycerol as cryoprotectant. Datasets were collected on beam line ×10SA at the Swiss Light Source (Paul Scherrer Institut, Villigen, Switzerland) and were indexed, integrated, and scaled with the XDS package. The model was built in COOT and refined with REFMAC5 using TLS- refinement (CCP4 suite). Figures were generated using PYMOL (DeLano Scientific LLC).

References:

(18) Herzig, M. C.; Kolly, C.; Persohn, E.; Theil, D.; Schweizer, T.; Hafner, T.; Stemmelen, C.; Troxler, T. J.; Schmid, P.; Danner, S.; Schnell, C. R.; Mueller, M.; Kinzel, B.; Grevot, A.; Bolognani, F.; Stirn, M.; Kuhn, R. R.; Kaupmann, K.; van der Putten, P. H.; Rovelli, G.; Shimshek, D. R. LRRK2 Protein Levels Are Determined by Kinase Function and Are Crucial for Kidney and Lung Homeostasis in Mice. *Hum. Mol. Genet.* **2011**, *20*, 4209–4223.

(19) Ness, D.; Ren, Z.; Gardai, S.; Sharpnack, D.; Johnson, V. J.; Brennan, R. J.; Brigham, E. F.; Olaharski, A. J. Leucine-Rich Repeat Kinase 2 (LRRK2)-Deficient Rats Exhibit Renal Tubule Injury and Perturbations in Metabolic and Immunological Homeostasis. *PLoS One* **2013**, *8*, e66164.

(20) Tong, Y.; Giaime, E.; Yamaguchi, H.; Ichimura, T.; Liu, Y.; Si, H.; Cai, H.; Bonventre, J. V; Shen, J. Loss of Leucine-Rich Repeat Kinase 2 Causes Age-Dependent Bi-Phasic Alterations of the Autophagy Pathway. *Mol. Neurodegener.* **2012**, *7*, 2.

Figure legend:

Fig.1: IC50 measurements of HG09-106-03 and HG09-105-05 on LRRK2 kinase. Phosphorylation of Ser 910/935 as readout.

Fig.2: Co-crystal structure of Roco4 kinase and HG09-106-03 A. Overlay of the AppCp (blue) with the HG09-106-03 (green) structure. B. Close-up of the inhibitor binding pocket. Hydrogen bonds indicated by dashed line. C. Chemical structure of HG09-106-03. D. Structure of HG09-106-03. Observed electron density indicated by mesh.

Fig.3: Co-crystal structure of Roco4 kinase and HG09-105-05. A. Overlay of the AppCp (blue) with the HG09-105-05 (green) structure. B. Close-up of the inhibitor binding pocket. Hydrogen bonds indicated by dashed line. C. Chemical structure of HG09-105-05. D. Structure of HG09-105-05. Observed electron density indicated by mesh.

Fig. 1

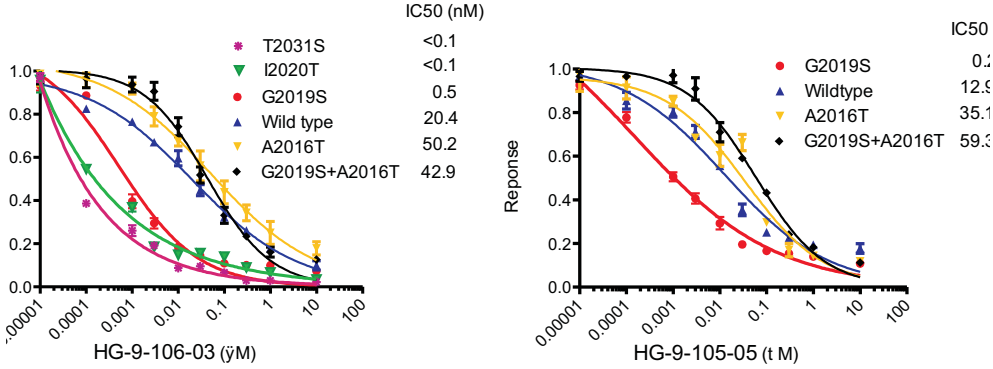
IC50 (nM)
T2031S <0.1
I2020T <0.1
G2019S 0.5
Wild type 20.4
A2016T 50.2
G2019S+A2016T 42.9
1.0
0.8
0.6
0.4
0.2
0.0
0.0001
0.001
0.01
0.1
1
10
100
HG-9-106-03 (ÿM)
IC50
G2019S
Wildtype
A2016T
G2019S+A2016T
Reponse
0.00001
0.0001
0.001
0.01
0.1
1
10
100
HG-9-105-05 (t M)

Fig. 2

A

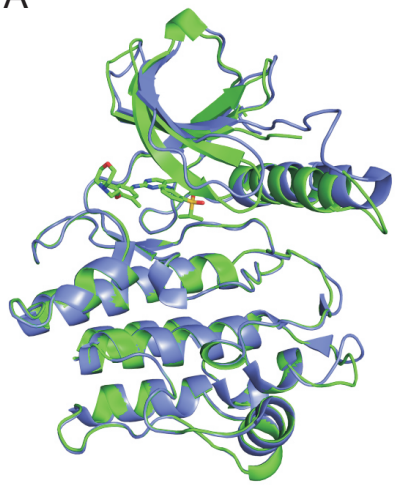

B

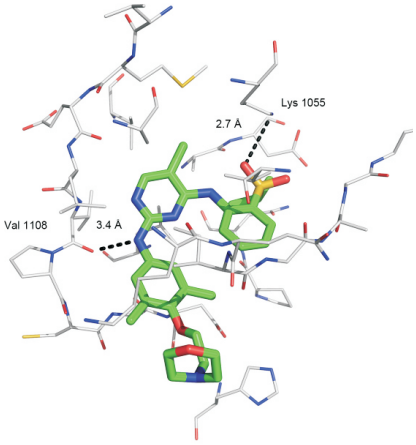

C

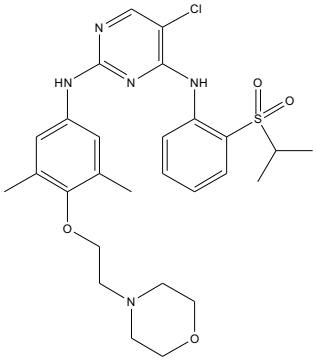

D

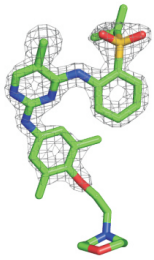

Fig. 3

A

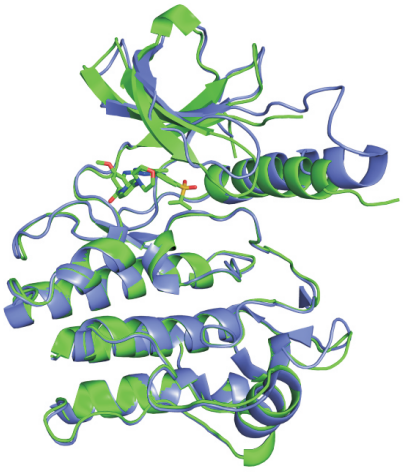

B

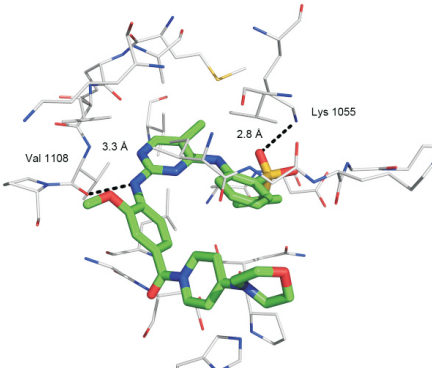

C

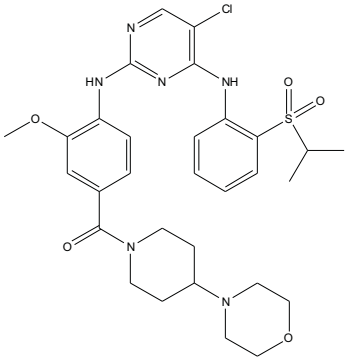

D